Strontium-Substituted Hydroxyapatite-Gelatin Biomimetic Scaffolds Modulate Bone Cell Response

Strontium-Substituted Hydroxyapatite-Gelatin Biomimetic Scaffolds Modulate Bone Cell Response

Silvia Panzavolta, Paola Torricelli, Sonia Casolari, Annapaola Parrilli, Milena Fini, and Adriana Bigi*

Strontium has a beneficial role on bone remodeling and is proposed for the treatment of pathologies associated to excessive bone resorption, such as osteoporosis. Herein, the possibility to utilize a biomimetic scaffold as strontium delivery system is explored. Porous 3D gelatin scaffolds containing about 30% of strontium substituted hydroxyapatite (SrHA) or pure hydroxyapatite (HA) are prepared by freeze-drying. The scaffolds display a very high open porosity, with an interconnectivity of 100%. Reinforcement with further amount of gelatin provokes a modest decrease of the average pore size, without reducing interconnectivity. Moreover, reinforced scaffolds display reduced water uptake ability and increased values of mechanical parameters when compared to as-prepared scaffolds. Strontium displays a sustained release in phosphate buffered saline: the quantities released after 14 d from as-prepared and reinforced scaffolds are just 14 and 18% of the initial content, respectively. Coculture of osteoblasts and osteoclasts shows that SrHA-containing scaffolds promote osteoblast viability and activity when compared to HA-containing scaffolds. On the other hand, osteoclastogenesis and osteoclast differentiation are significantly inhibited on SrHA-containing scaffolds, suggesting that these systems could be usefully applied for local delivery of strontium in loci characterized by excessive bone resorption.

1. Introduction

Strontium is a trace element in the human body, where it plays an important biological role. As other bone seeking elements, it is taken up by recent mineral deposits.[1] In fact, its presence is greater in the regions of high metabolic turnover and increases on passing from old to new bone, reaching values up to about 2.5-fold higher in cancellous bone and 3–4-folds higher in compact bone.[1,2] Its beneficial influence on bone remodeling has been ascribed to the combined effect of decrease of bone resorption and enhancement of bone formation.[3,4] In vitro and in vivo studies demonstrate that Sr is able to increase the number and activity of osteoblast, whereas it inhibits osteoclastogenesis and osteoclast differentiation.[5,6] Furthermore, clinical studies show a beneficial effect of strontium treatment in osteoporotic patients.[5,7–9]

These positive results have stimulated a growing interest toward calcium phosphates bioceramics, coatings, and cements as possible delivery systems of Sr ion.[10–15] In particular, Sr has been shown to stimulate viability and differentiation of osteoblast and to hinder osteoclast proliferation and activity in a dose-dependent way,[16–21] and to promote implant integration in ovariectomized rats,[18] also when incorporated into hydroxyapatite (HA) structure. A few studies also proposed the use of Sr-doped/substituted HA, either alone or in combination with polysaccharides, for the preparation of porous scaffolds.[22–25]

In this work, we explored the possibility to utilize a biomimetic scaffold as delivery system for Sr ion. To this aim, we developed porous gelatin based scaffolds enriched with Sr-substituted HA (SrHA). Porosity is a mandatory requirement of scaffolds for regenerative medicine in order to favor cell migration, as well as nutrient and waste exchange.[26–28] 3D porous scaffolds were prepared by freeze-drying gelatin foams. Although gelatin is widely applied in the biomedical field, thanks to its abundance, low cost, lack of antigenicity, excellent biocompatibility and biodegradability, its high solubility in aqueous solution constitutes a major drawback. As a consequence, gelatin-based biomaterials must be stabilized against dissolution in solution. To this purpose, we cross-linked the foamed scaffolds with glutaraldehyde at relatively low concentration, which does not provoke any cytotoxic effect.[29,30]

Calcium and strontium belong to the same group of the periodic table of elements and exhibit a similar chemical behavior. Thus, it is not surprising that Sr can replace Ca in hydroxyapatite in the whole range of composition. The substitution provokes an expansion of the unit cell due to the bigger dimensions of Sr^{2+} (ionic radius: 1.20 Å) than Ca^{2+} (ionic radius: 0.99 Å)[31,32] and modifies the solubility of hydroxyapatite, which increases with strontium content.[33,34] In this study, the choice of the degree

Dr. S. Panzavolta, Dr. S. Casolari, Prof. A. Bigi
Department of Chemistry "G. Ciamician"
University of Bologna
via Selmi, 2, Bologna 40126, Italy
E-mail: silvia.panzavolta@unibo.it
Dr. P. Torricelli, Dr. A. Parrilli, Dr. M. Fini
Laboratory of Preclinical and Surgical Studies
IRCCS Rizzoli Orthopaedic Institute
via di Barbiano 1/10, 40136 Bologna, Italy

of Sr substitution in SrHA utilized for the preparation of the scaffolds was based on the results of previous in vitro studies, which demonstrated that Sr substitution of a few atom% is able to influence bone cells behavior reducing osteoclast activity and promoting osteoblast differentiation.[17,18] Moreover, some of the scaffolds were reinforced through addition of a proper amount of gelatin,[35] in order to modulate strontium release. Viability and activity of bone cells were evaluated using cocultures of osteoblasts and osteoclasts. In particular, the influence of strontium on differentiation markers was evaluated both through immunoenzymatic assay and by means of quantitative polymerase chain reaction (qPCR).

2. Experimental Section

Type A gelatin (300 Bloom, from pig skin) and glutaraldehyde (25% w/v aqueous solution) were purchased from Sigma. Genipin was purchased from Wako Chemicals. HA and Sr-substituted HA were obtained through direct synthesis in aqueous solution. Briefly, 50 mL of 0.65 M $(NH_4)_2HPO_4$ solution, pH 10 adjusted with NH_4OH, was added dropwise under stirring to the 1.08 M cationic solution ($Ca(NO_3)_2 \cdot 4H_2O$ and $Ca(NO_3)_2 \cdot 4H_2O + Sr(NO_3)_2$, with a Sr/(Ca + Sr) ratio of 0.00 and 0.10 for HA and SrHA, respectively), heated at 90 °C. The obtained solid products were centrifuged, dried at 37 °C, finely ground in a mortar and sieved <80 μm before use.

2.1. Scaffolds Preparation

Gelatin-based scaffolds were prepared starting from a 10% w/v aqueous gelatin solution, as described in literature.[30] 30 g of gelatin were dissolved in 300 mL of distilled water at 55 °C, then 13 g of HA or Sr-HA (30% w/w) were added. The suspension was mechanically stirred (≈600 rpm) for about 5 min to obtain white foam. The foam was deposited on waxed paper, allowed to gelify at 20 °C for 2 h, cut into the desired shapes, rinsed in ethanol and freeze-dried for 24 h at −44 °C and 0.1 mbar. Freeze-dried samples were soaked in a 0.3% (w/v) glutaraldehyde solution in EtOH for 6 h, washed in 0.1 M glycine aqueous solution for 30 min, and rinsed twice in distilled water. Afterward, the scaffolds were soaked in ethanol for few minutes, and then freeze-dried for 24 h at −44 °C and 0.1 mbar. The obtained scaffolds were labeled as G_HA and G_SrHA.

In order to improve mechanical properties and modify the in vitro performance of the scaffolds,[35] the samples were reinforced with a 10% (w/v) gelatin solution containing 0.15% (w/v) of genipin. To this aim, samples (about 1 × 1 × 1 cm, weight ≈ 50 mg) were soaked into 10 mL of genipin/gelatin solution for 5 min and then freeze-dried (24 h at −44 °C and 0.1 mbar).

The reinforced scaffolds were labeled as G_HA_G and G_SrHA_G.

2.2. Scaffolds Characterization

The synthesized inorganic phases were characterized by powder X-ray diffraction (XRD) analysis. XRD patterns were recorded using a PANalytical powder diffractometer equipped with a fast X'celerator detector. CuKα radiation was used (40 mA, 40 kV). The 2θ range was from 5° to 50° with a step size of 0.033° and time per step of 10 s. To evaluate the coherence lengths of crystalline domains, further X-ray powder data were collected with a fixed counting time of 400 s for each 0.033 step^{-1}. Silicon was used as internal standard. The coherence lengths of crystalline domains were calculated according to the Scherrer formula.[31]

Transmission electron microscopy (TEM) investigation of the synthesized powders was carried out using a Philips CM 100 transmission electron microscope operating at 80 kV. A small amount of powder was dispersed in ethanol and submitted to ultrasonication. A drop of the suspension was transferred onto holey carbon foils supported on conventional copper microgrids.

Mechanical characterization of the scaffolds was performed on 1 × 1 × 1 cm samples. Compression tests were carried out using a 4465 Instron testing machine, equipped with a 1 kN load cell. Ten samples were tested for each composition, at a loading rate of 1.0 mm min^{-1}. Statistical analysis was performed with the Student *t*-test considering a *P*-value of less than 0.05 to be significantly different.

The morphology of the scaffolds, sputter-coated with gold, was observed using a Philips XL-20 scanning electron microscope with a 15 kV accelerating voltage.

The amount of adsorbed gelatin on reinforced scaffolds was calculated as

$$W\% = \frac{(W_A - W_B) \times 100}{W_B} \quad (1)$$

where W_B and W_A are the weights of the sample before and after reinforcement. ≈20 samples were prepared and weighted for each composition.

The equilibrium water uptake ability (WUA) was determined after immersion of the preweighted dry samples in phosphate buffered saline (PBS) 0.1 M, pH 7.4 at 37 °C for 20 s. The weight of wet samples was measured after PBS excess removal. Then, the water uptake ability was calculated according to the following equation

$$\mathrm{WUA} = \frac{W_w - W_d}{W_d} \quad (2)$$

where W_w and W_d represent the weight of wet and dry sample, respectively.[35] The process was repeated in triplicate and data were reported as mean and standard deviation. For the evaluation of strontium release kinetics, G_SrHA and G_SrHA_G samples were weighted, immersed in 10 mL of saline solution (NaCl 0.9% in ultrapure water, added with sodium azide in order to prevent microbial contamination) and stored at 37 °C for different periods of time. At the end of every selected time the medium was completely removed. Three different samples for each time were analyzed. Aliquots of the collected medium were suitably diluted with HNO_3 Ultrapure 0.5M, containing 10% (m/v) of $LaCl_3 \cdot xH_2O$ (99% trace metal basis, Aldrich), and quantitative determination of strontium content was made by means of atomic absorption spectrophotometer (AAS, Perkin Elmer Analyst 400) equipped with an air-acetylene burner and

a strontium lamp working at a wavelength of 460.73 nm. The standard additions method was used.

2.3. μCT Analysis

Five samples of each type (G_HA, G_SrHA, G_HA_G, and G_SrHA_G) were scanned with the Skyscan 1172 μCT system (Bruker-MicroCT, Belgium) applying a voltage of 60 kV and a current of 170 μA. Each sample rotated 180° with a rotation step of 0.3° and the resulted scanning images had a nominal resolution of 5 μm (2096 × 4000 pixels). Afterward, the NRecon program (version 1.7.1.6, Bruker) was used for the tomographic reconstruction in order to obtain μCT sections (4000 × 4000 pixels, maintaining the relative pixel size). In addition to the specific alignment relative to each single scan, a reduction of the ring artifacts was used as correction factor for the reconstruction process.

The quantitative morphometric analysis on μCT datasets was carried out using CTAn software (version 1.17.7.2, Bruker). A cubic volume of interest (VOI) of 3 × 3 × 3 mm was defined in each sample. Then the following 3D parameters related to the material porosity were calculated

- the closed porosity P.cl (%), defined as the ratio between the volume of the closed and not 3D interconnected pores detected in the scaffolds and the total volume (VOI);
- the open porosity P.op (%), defined as the ratio between the volume of the open and 3D interconnected pores detected in the scaffolds and the total volume (VOI);
- the porosity P.tot (%), defined as the ratio between the volume of the pores detected in the scaffolds and the total volume (VOI);
- pore connection (%), calculated through an individual 3D analysis using the following formula

$$\frac{V_{\max} \text{ detected pore}}{\sum V_{\text{tot}} \text{ detected pores}} \times 100 \quad (3)$$

Moreover, in the same VOI, a 2D analysis of porosity distribution was carried out calculating both the diameter (P.ECDa in mm) of the circle having the same area as the single measured pore detected in each tomographic section and the percentage of 2D porosity $P(tot)A_i$ along the whole thickness of the scaffolds.

2.4. In Vitro Coculture Model

The coculture model was performed with human osteoblast-like cells MG63 (OB, Istituto Zooprofilattico Sperimentale IZSBS, Brescia, Italy) and human osteoclast precursor 2T-110 (OC, Poietics Osteoclast Precursor Cell System, Lonza Walkersville, Inc., MD, USA).

OB were previously expanded in Dulbecco's modified Eagle medium (DMEM) supplemented with 10% FCS, 1% antibiotics (100 U mL^{-1} penicillin, 100 μg mL^{-1} streptomycin), β-glycerolphosphate (10^{-4} M), and ascorbic acid (50 μg mL^{-1}), counted, seeded at a concentration of 2×10^4 cells/well onto the different samples (G_HA, G_SrHA, G_HA_G, G_SrHA_G).

Pre-osteoclasts were plated at a concentration of 3×10^4 cells/well in the bottom of 24-wells plates cultured in DMEM added with macrophage colony-stimulating factor (MCSF, 25 ng mL^{-1}) and receptor activator for κB factor ligand (RANKL, 30 ng mL^{-1}) in standard condition, at 37 °C ± 0.5 with 95% humidity and 5% CO_2 ± 0.2 to activate cell differentiation.

After 24 h from seeding, material samples with OB were cocultured in the same wells with OC. Medium was a mixture of each cell type medium according to cell density proportion.

2.4.1. Cells Viability and Morphology

Cocultured OB and OC were separately evaluated for viability and proliferation on disassembled cocultures, transferring samples with OB in empty wells, by WST1 colorimetric reagent test (Roche Diagnostics GmbH, Manheim, Germany) at the end of experimental time. The assay is based on the reduction of tetrazolium salt to a soluble formazan salt by a reductase of the mitochondrial respiratory chain, active only in viable cells. 100 μL of WST1 solution and 900 μL of medium (final dilution: 1:10) were added to wells containing OC or OB, and the multiwell plates were incubated at 37 °C for the next 4 h. Supernatants were quantified spectrophotometrically at 450 nm with a reference wavelength of 625 nm. Results of WST1 are reported as optical density (OD) and directly correlated with the cell number.

At 7 d OB and OC viability and morphology were also observed by the Live/Dead assay (Molecular Probes, Eugene, OR), according to the manufacturer's instructions. Samples were visualized using an inverted microscope equipped with an epifluorescence setup (Eclipse TiU, NIKON Europe BV, NITAL SpA, Milan, Italy): excitation/emission setting of 488/530 nm to detect green fluorescence (live cells) and 530/580 nm to detect red fluorescence (dead cells).

2.4.2. Osteoclast Differentiation

TRAP (tartrate-resistant acid phosphatase) staining was performed, after 14 d of coculture, to assess osteoclast differentiation starting from mononucleated cells, according to manufacturer's instructions (SIGMA, Buchs, Switzerland). The positive cells developed red color of different intensity. Osteoclastogenesis was evaluated by counting the number of TRAP-positive multinucleated cells (three or more nuclei each cell), under the microscope by a semiautomatic software (NIS-Elements AR 4.30.01). Results are given as percentage of OC control culture (HA) considered as 100%.

2.4.3. qPCR

Total RNA was extracted from all samples at the end of experimental time using PureLink RNA Mini Kit (Life Technologies, Carlsbad, CA). Purified RNA was reverse transcribed with Superscript VILO cDNA Synthesis kit (Invitrogen, Life Technologies,

Table 1. Specifications of primer used for qPCR analysis.

GENE	Primer forward	Primer reverse	Amplicon length	Annealing temperature
GAPDH	5′-TGGTATCGTGGAAGGACTCA-3′	5′-GCAGGGATGATGTTCTGGA-3′	123 bp	56 °C
ALPL	QuantiTect Primer Assay (Qiagen) Hs_ALPL_1_SG		110 bp	55 °C
BGLAP	QuantiTect Primer Assay (Qiagen) Hs_BGLAP_1_SG		90 bp	55 °C
CASP3	QuantiTect Primer Assay (Qiagen) Hs_CASP3_1_SG		147 bp	55 °C
COL1A1	QuantiTect Primer Assay (Qiagen) Hs_COL1A1_1_SG		118 bp	55 °C
CTSK	CAGACAACAGATTTCCATCAGC	CTTCTTCCATAGCTCCCAGTG	118 bp	60 °C
OPG	CTACCAAGACACTAAGCCAGT	AAACAGTGAATCAACTCAAAAATGTG	113 bp	60 °C
RANKL	TGAGATGAGCAAAAGGCTGAG	AGGAGCTGTGCAAAAGGAAT	134 bp	60 °C

Carlsbad, CA), following manufacturer's instructions. Each sample (10 ng) was tested in duplicate. qPCR analysis was performed in a LightCycler Instrument (Roche Diagnostics GmbH, Mannheim, Germany) using the QuantiTect SYBR Green PCR kit (Qiagen, Hilden, Germany). The protocol included a denaturation at 95 °C for 15′, 40 cycles of amplification (95 °C 15″, appropriate annealing temperature for each target as detailed in **Table 1** for 20″ and 72 °C for 20″) and a melting curve to check for amplicon specificity. The threshold cycle was used for the calculation of relative expression by means of the 2-ΔΔCt method against GAPDH as reference gene, and HA samples as calibrator. Studied genes are summarized in Table 1.

2.4.4. Immunoenzymatic Assays

At the end of experimental times, after 7 and 14 d of culture, the supernatant was collected from all wells and centrifuged to remove particulates, if any. Aliquots of supernatant were dispensed in Eppendorf tubes for storage at −70 °C and assayed with the following immunoenzymatic kits: alkaline phosphatase (ALP), CloudClone Corp., Wuhan, China), collagen type I (COLL1, CloudClone), osteoprotegerin (OPG, CloudClone), and receptor activator for nuclear factor KB ligand (RANKL, CloudClone).

2.4.5. Statistical Analysis

Statistical evaluation of data was performed using the software package SPSS/PC+ Statistics 23.0 (SPSS Inc., Chicago, IL). The results presented are the mean of six independent values. Data are reported as mean ± standard deviations (SD) at a significance level of $p < 0.05$. After having verified normal distribution and homogeneity of variance, a one-way ANOVA was done for comparison between groups. Finally, a post hoc multiple comparison test was performed to detect significant differences among groups.

3. Results and Discussion

3.1. Scaffolds Characterization

3D porous gelatin scaffolds were enriched with SrHA with the aim to obtaining systems able to sum up the good biological performance of gelatin and hydroxyapatite with the anti-osteoporotic activity of strontium. The X-ray powder diffraction pattern of the synthesized SrHA displays a number of peaks characteristic of hydroxyapatite, which results in the only crystalline phase. The main diffraction peaks of SrHA are slightly shifted at lower angles when compared to those present in the X-ray diffraction pattern of the sample synthesized in the absence of strontium (HA), as shown in Figure S1a (Supporting Information). In particular, the (002) reflection is shifted of 0.102° of 2θ, as shown in Figure S1b (Supporting Information). In agreement, the lattice constants of SrHA are $a = 9.4638(8)$ Å, $c = 6.9180(7)$ Å, which are slightly greater than those of HA, $a = 9.4271$ (1) Å, $c = 6.8815(9)$ Å and indicate a partial substitution of the bigger strontium ion for calcium in the structure of hydroxyapatite. The enlarged unit cell of SrHA is coherent with the content of Sr, which is 8 at%, as measured through AAS. In agreement with previous data,[31] incorporation of Sr into hydroxyapatite structure also provokes a reduction of the coherent length of the perfect crystalline domains (τ_{hkl}), as appears from the slightly broader XRD peaks of SrHA than HA. The values of the crystalline domains, calculated using the Scherrer method in the direction normal to 002 and 310 planes, are 32 ± 2 and 12 ± 2 nm for SrHA, and 35 ± 2 and 21 ± 2 nm for HA. Moreover, SrHA nanocrystals display reduced mean dimensions and more perturbed shapes when compared to HA nanocrystals (Figure S2, Supporting Information).

The inorganic phase content of the scaffolds is 30 wt% both for G_HA and G_SrHA, as verified by thermogravimetric analyses (data not shown). The results of μ-CT analysis confirm the high porosity of the scaffolds. Both macro and microporosity are appreciable in the 3D reconstructed images and in the cross-sectional scanning electron microscopy (SEM) images reported in **Figure 1**c. The values of porosity (i.e., the percentage of void space in a solid) are slightly different for G_HA and G_SrHA, but however very high, with 100% pore interconnectivity (**Table 2**).

The slightly smaller value of open porosity measured for G_SrHA might be related to the relatively smaller dimensions of SrHA than HA crystals, which also results in a finer dispersion of the inorganic particles inside the G_SrHA scaffold than within G_HA (Figure 1b). Both types of scaffold present a broad pore size distribution (**Figure 2**) with a large maximum centered around 300–400 and 250–350 μm for G_HA and G_SrHA, respectively. It is worthwhile to remember that the minimum pore size required for cell migration and transport

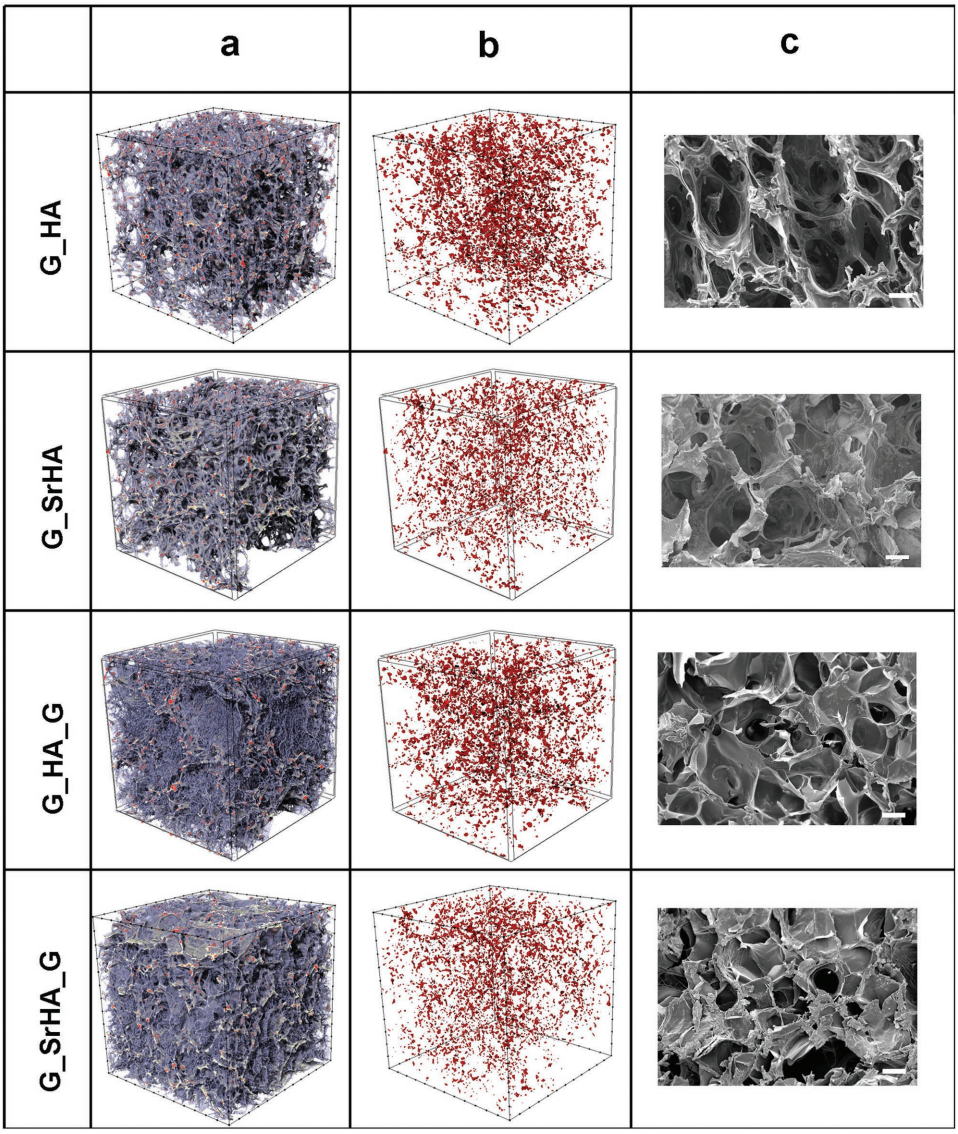

Figure 1. 3D μ-CT representation and SEM images of the different samples. a) 3D models of the scaffolds and b) their inorganic phase (red) distribution; c) SEM images. Scale bars = 200 μm.

and significant bone growth is about 100 μm, whereas larger pores can lead to direct osteogenesis.[36,37]

Reinforcement with gelatin provokes a slight reduction of the total porosity, as results from the comparison of the μCT data obtained for G_HA and G_SrHA with those of G_HA_G and G_SrHA_G, respectively, but it does not affect pore interconnectivity, which is still 100% (Table 2). Reinforcement provokes a major influence on pore size distribution. In fact, the curves described by the pore size distributions (Figure 2) appear sharper and shifted toward smaller pore sizes when compared to those of the as-prepared scaffolds. A great part of the pores in G_HA_G and G_SrHA_G displays sizes between 100 and 300 μm, with a maximum around 200 μm. All as-prepared and reinforced scaffolds display a homogeneous distribution of porosity along their whole thickness, as it can be appreciated in Figure S3 (Supporting Information).

Table 2. Porosity parameters of the different scaffolds.

	G_HA	G_SrHA	G_HA_G	G_SrHA_G
P.cl [%]	0.00 ± 0.00	0.00 ± 0.00	0.00 ± 0.00	0.00 ± 0.00
P.op [%]	93.94 ± 0.26	91.74 ± 0.52	91.38 ± 1.02	88.97 ± 1.06
P.tot [%]	93.94 ± 0.26	91.74 ± 0.52	91.38 ± 1.02	88.97 ± 1.06
P.conn [%]	100.00 ± 0.00	100.00 ± 0.00	100.00 ± 0.00	100.00 ± 0.00

The amount of gelatin adsorbed on reinforced samples is reported in **Table 3**: the value is around 160% of the initial weight of the samples for G_SrHA and slightly higher for G_HA. These values fit very well to the different porosity exhibited by the scaffolds after reinforcement and are responsible of the drastic reduction of the water uptake ability. The as-prepared scaffolds exhibit very high values of WUA, whereas, after reinforcement, the WUA values are about one order of magnitude smaller than those of as-prepared samples (Table 3).

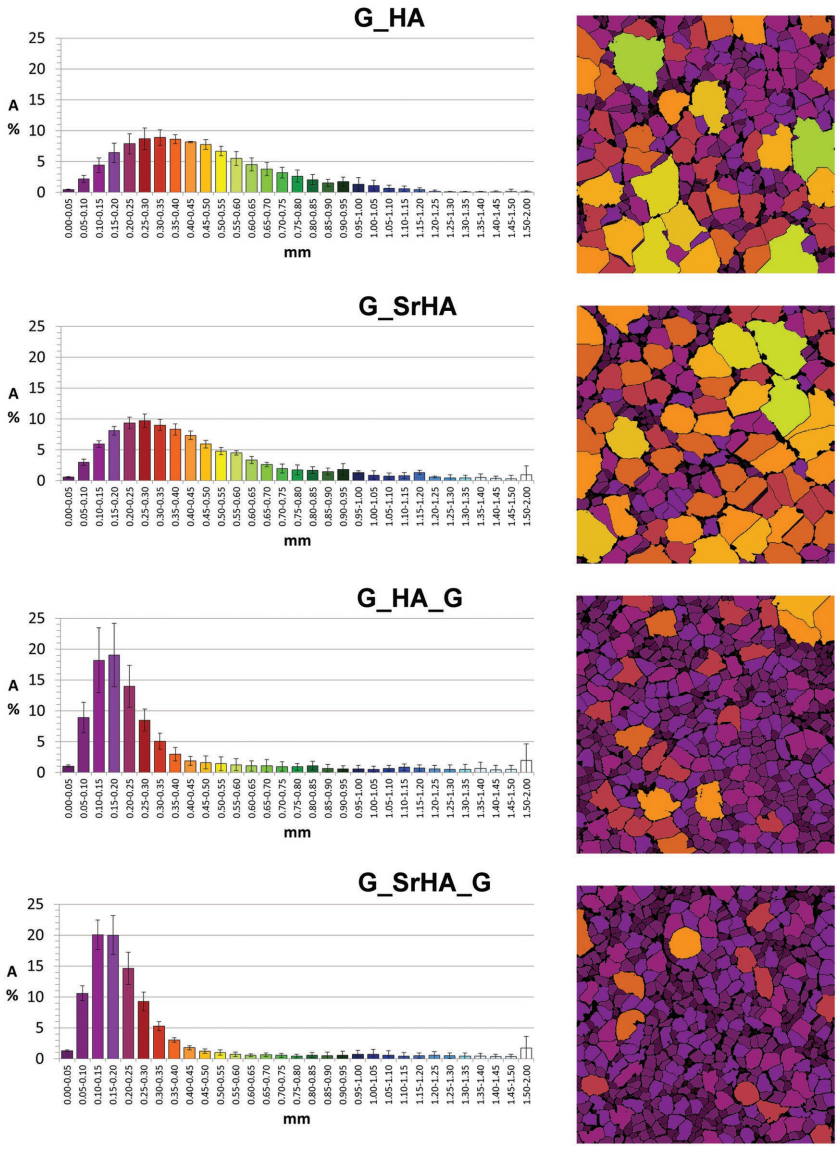

Figure 2. Left: histograms of pore size distribution P.ECD reported as the diameters (mm) grouped in different intervals of magnitude (*x*-axis) compared to the percentage of area occupied (*y*-axis), and right, 2D μ-CT sections of the scaffold pores colored using the same color code of the P.ECD histograms.

The decrease is most likely ascribable to the stiffening of the scaffolds caused by gelatin crosslinking induced by the presence of genipin in the reinforcement solution. The different values of WUA obtained for HA and SrHA-containing scaffolds are in agreement with the different values of open porosity and pore size distribution recorded for the two types of scaffold.

The compressive stress–strain curves of the scaffolds are reported in Figure S4 (Supporting Information). Three distinct zones, which correspond to linear elastic, collapse plateau, and densification regimes,[37] can be appreciated in the curves.

The values of elastic modulus (E), determined via linear regression of the initial linear regime, the collapse stress (σ), and strain (ε), determined by the intersection point of the linear line for calculation of E and the linear regression of the collapse plateau regime ($\Delta\sigma/\Delta\varepsilon$) are reported in **Figure 3**. All the mechanical parameters obtained for G_SrHA exhibit slightly reduced values when compared to those of G_HA, although the differences are not statistically significant ($p > 0.05$). Moreover, the values of elastic modulus and stress of reinforced scaffolds are much higher than those of as-prepared scaffolds. These results are in agreement with previous data[35] that demonstrated that gelatin adsorption onto porous scaffolds enhanced both the values of stress and elastic modulus, acting as a stiffening agent. The improved mechanical properties can be ascribed to the reduction of pores size caused by gelatin reinforcement and to the formation of additional crosslinks involving genipin and gelatin scaffold.[38]

The scaffolds show a good stability in solution, confirmed by the measurements of gelatin cumulative release: as a matter of fact, the values recorded for as-prepared scaffolds amount to just 4 wt% after 7 d in PBS, whereas in the same period of time release from reinforced samples reaches values around 14 wt%.

Furthermore, the amount of strontium released as a function of soaking time in PBS was evaluated and reported in **Figure 4**, where it is possible to appreciate that release increases with time up to about 10 d, after which it reaches a steady state (Figure 4).

The cumulative release of strontium reaches values of about 14 and 18% of the initial content for as-prepared and reinforced scaffolds, respectively. The greater amount of strontium released from reinforced scaffolds could be due to the process of reinforcement, which is performed using a genipin–gelatin solution, which has a pH of about 5.5. The substitution of Sr for Ca in hydroxyapatite structure, even at relatively low percentage, provokes a significant increase of solubility and a shift of the solubility isotherms at higher pH.[33] It can be suggested that immersion in the acidic reinforcement solution provokes a partial dissolution of SrHA, which diffuses in the reinforcing material and can be more easily released in solution.

Table 3. Values of weight increase (%) of the scaffolds after reinforcement with gelatin and of water uptake ability (WUA).

	Weight increase [%]	WUA [g PBS g^{-1} sample]
G_HA	170 ± 10	20 ± 3
G_SrHA	160 ± 5	16 ± 2
G_HA_G		4 ± 1
G_SrHA_G		2 ± 0.2

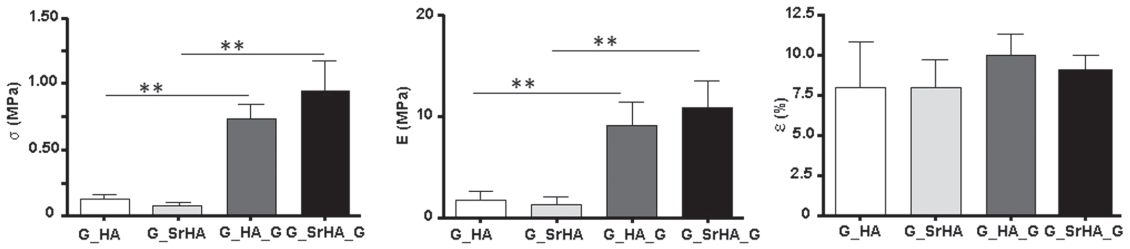

Figure 3. Mean values of collapse stress (σ), linear elastic modulus (E), and strain (ε%) of the different scaffolds. Each value is the mean of six determinations and is reported with its standard deviation. (**$p < 0.001$) Stress: **G_HA versus G_HA_G; G_SrHA versus G_SrHA_G Elastic modulus: **G_HA versus G_HA_G; G_SrHA versus G_SrHA_G.

3.2. Osteoblast and Osteoclast Viability and Morphology

The results of WST1 test indicate that osteoblasts grew regularly on all biomaterials (**Figure 5**a).

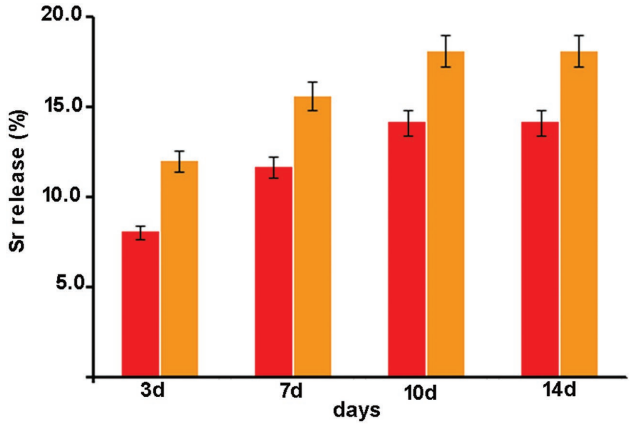

Figure 4. Strontium cumulative release from G_SrHA (red) and G_SrHA_G (orange) as a function of soaking time in PBS solution.

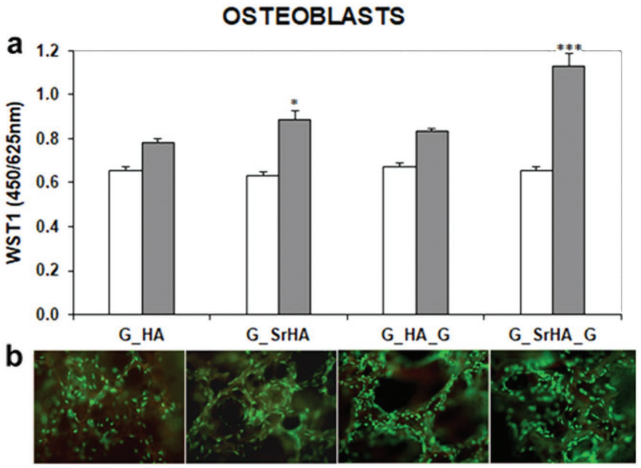

Figure 5. Osteoblast viability and morphology after cocolture with osteoclast on the different samples. a) Osteoblast proliferation after 7 (light bars) and 14 (dark bars) by WST1 reagent test. Statistical analysis is reported in the figure (*$p < 0.05$, **$p < 0.005$, ***$p < 0.0005$): *G_SrHA versus G_HA; *** G_SrHA_G versus G_HA, G_HA_G, G_SrHA. b) Live&Dead significant images of osteoblast grown on material samples (magnification 10×).

At 7 d no differences were found among groups. At 14 d values on G_SrHA were significantly higher when compared to G_HA, and G_SrHA_G was significantly higher in comparison to all other groups. Live&Dead staining (Figure 5b) showed that osteoblast colonization inside the scaffolds was consistent with osteoblast viability values. Cells appeared well spread and adherent onto material surface, and showed a normal morphology. Reinforcement with gelatin did not affect osteoblast adhesion to HA-containing scaffolds.

SrHA-containing samples displayed increased cell viability and adhesion both in as-prepared scaffolds and, even more, in reinforced scaffolds, probably due to a greater release of Sr and, as a consequence, to a higher availability of Sr in culture medium. In fact, it was found that Sr increases bone formation stimulating osteoblast proliferation through the activation of different cellular signaling pathway associated to Ca-sensing receptor.[39]

WST1 test and Live&Dead staining (**Figure 6**a,b) data show that osteoclasts grew normally in presence of G_HA and

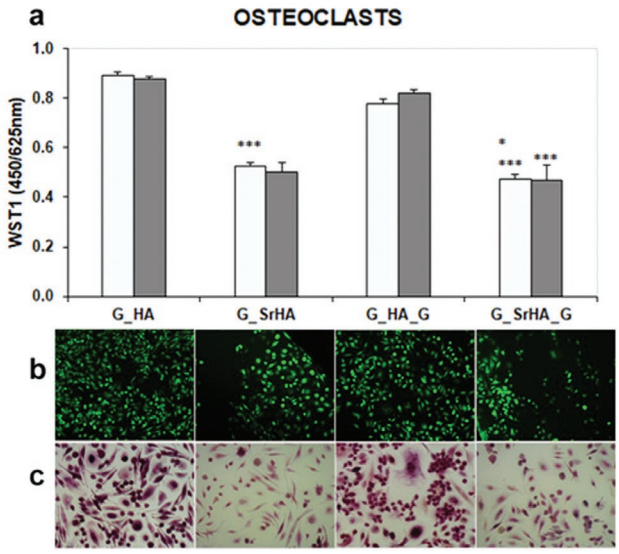

Figure 6. Osteoclast viability and differentiation after cocolture with osteoblast on the different samples. a) Osteoclast viability after 7 (light bars) and 14 (dark bars) days of culture by WST1 reagent test. Statistical analysis is reported in the figure (*$p < 0.05$, **$p < 0.005$, ***$p < 0.0005$): 7 d, * G_SrHA_G versus G_SrHA; 7 and 14 d *** G_SrHA, G_SrHA_G versus G_HA, G_HA_G. b) Live&Dead significant images of osteoclasts grown around material samples (magnification 10×). c) TRAP staining of osteoclasts (magnification 20×) after 14 d of coculture with osteoblast: considering G_HA as 100%, G_SrHA, G_HA_G, and G_SrHA_G were 32, 89, and 24%, respectively.

G_HA_G, whereas their number decreased significantly at both 7 and 14 d on SrHA-containing scaffolds.

TRAP staining (Figure 6c) shows that monocytes, under the action of RANKL and MSCF, changed their morphology and aggregated into very large polynucleated cells typical of differentiated osteoclasts. Not only viability but also monocytes differentiation in active cells was affected by the presence of SrHA, as demonstrated by TRAP staining: a smaller percentage of multinucleated cells was counted in G_SrHA and G_SrHA_G groups than in G_HA and G_HA_G, as shown in Figure 6c.

3.3. Osteoblast and Osteoclast Activity

Gene expression of some common markers of osteoblast activity, such as ALPL (alkaline phosphatase), COL1A1 (collagen type I), and BGLAP (osteocalcin) was assessed at 7 and 14 d of culture, in order to evaluate if osteoblast maintained their differentiation when cocultured with scaffolds. Results are summarized in **Figure 7**.

At 7 d ALPL was significantly lower in all groups when compared to HA, but at 14 d the activity of ALPL gene was particularly enhanced in osteoblasts on SrHA-containing scaffolds.

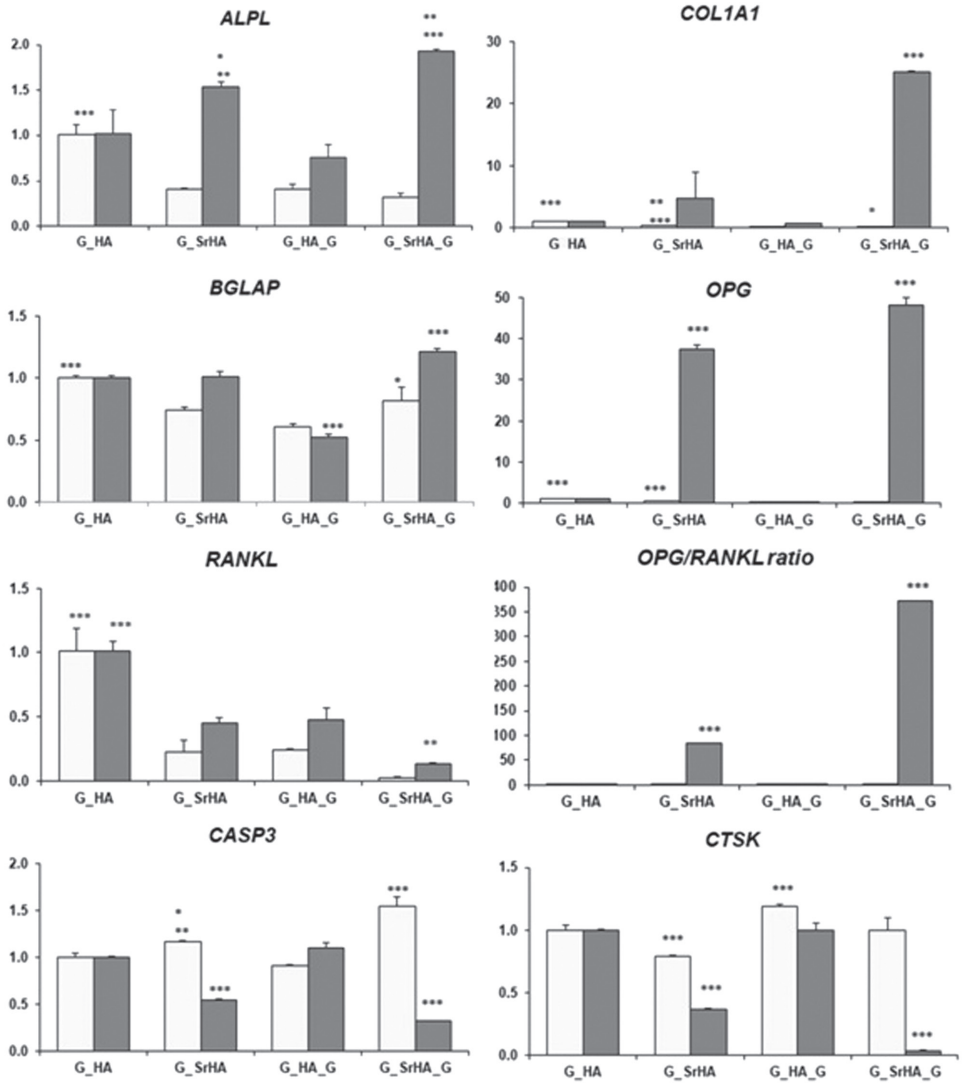

Figure 7. Gene expression of osteoblasts and osteoclast coculture onto the different samples after 7 and 14 d of culture. Statistical analysis is reported in the figure (*$p < 0.05$, **$p < 0.005$, ***$p < 0.0005$). ALPL. 7 days: ***G_HA versus G_SrHA, G_HA_G, G_SrHA_G; 14 d: *G_SrHA versus G_HA; **G_SrHA versus G_HA_G; **G_SrHA_G versus G_HA; ***G_SrHA_G versus G_HA_G. COL1A1. 7 d: ***G_HA versus G_SrHA, G_HA_G, G_SrHA_G; **G_SrHA versus G_SrHA_G; ***G_SrHA versus G_HA_G; *G_SrHA_G versus G_HA_G; 14 d: ***G_SrHA_G versus G_HA, G_SrHA, G_HA_G. BGLAP. 7 d. ***G_HA versus G_SrHA, G_HA_G, G_SrHA_G; *G_SrHA_G versus G_HA_G; 14 d. ***G_HA_G versus G_HA, GSrHA, G_SrHA_G; ***G_SrHA_G versus G_HA, G_SrHA. OPG. 7 d: ***G_HA versus G_SrHA, G_HA_G, G_SrHA_G; ***G_SrHA versus G_HA_G, G_SrHA_G; 14 d: ***G_SrHA versus G_HA, G_HA_G; ***G_SrHA_G versus G_HA, G_SrHA, G_HA_G. RANKL. 7 d: ***G_HA versus G_SrHA, G_HA_G, G_SrHA_G; 14 d: ***G_HA versus G_SrHA, G_HA_G, G_SrHA_G; **G_SrHA_G versus G_SrHA, G_HA_G. OPG/RANKL ratio. 14 d: ***G_SrHA, G_SrHA_G versus G_HA, G_HA_G. CASP3. 7 d: *G_SrHA versus G_HA; **G_SrHA versus G_HA_G; ***G_SrHA_G versus G_HA, G_SrHA, G_HA; 14 d: ***G_SrHA versus G_HA, G_HA_G; ***G_SrHA_G versus G_HA, G_SrHA, G_HA_G. CTSK. 7 d: ***G_HA_G versus G_HA, G_SrHA, G_SrHA_G; ***G_SrHA versus G_HA, G_SrHA_G; 14 d: ***G_SrHA versus G_HA, G_HA_G; ***G_SrHA_G versus G_HA, G_SrHA, G_HA_G.

COL1A1 expression was extremely low at 7 d in all groups and also remained low at 14 d in G_HA, G_SrHA, and G_HA_G groups. On the contrary, osteoblasts onto G_SrHA_G expressed a very high COL1A1 gene, when compared to all other groups.

BGLAP gene expression for the production of osteocalcin in the phase of tissue mineralization showed the highest values at 7 d in G_HA and G_SrHA_G, whereas at 14 d it was significantly higher in G_SrHA_G when compared to other groups, confirming higher expression of mineralization process in G_SrHA_G group.

The interaction between cells and biomaterials, in relation to the effects of osteoblast–osteoclasts coculture, was investigated through evaluation of the expression of OPG and RANKL, as representative of cell interplay in the balance between bone deposition and resorption. OPG at 7 d was expressed at low level in all groups; at 14 d it remain low in G_HA and G_HA_G groups, while it was strongly enhanced at 14 d in both SrHA-containing groups, which displayed reduced RANKL values, as shown in Figure 7. As a consequence, the OPG/RANKL ratio was significantly higher in G_SrHA and G_SrHA_G groups (83 and 373, respectively) than in G_HA (considered as 1) and G_HA_G (0.7).

OPG displays a regulatory activity on RANKL, blocking osteoclast formation, and is also responsible for the induction of apoptosis in mature osteoclasts. CASP3, whose activity is involved in the apoptosis pathway, showed a significant activation at 7 d, followed by a significant decrease at 14 d in G_SrHA and G_SrHA_G groups (Figure 7). The activity of CASP3 seems to be related to osteoclasts viability decrease, significant lowering in presence of Sr in the scaffold. These results are consistent with proliferation data.

CTSK is expressed by osteoclasts and its concentration is proportional to osteoclast activity in the bone resorption process. At 7 d, high values were detected in all groups, but G_SrHA showed significantly lower values when compared to others. At 14 d a significant decrease of gene expression was found in both SrHA-containing scaffolds, in agreement with other data of the present study on osteoclasts behavior.

The immunoenzymatic measure of some representative parameters in the culture supernatants gave results in agreement with qPCR data (**Figure 8**).

Both ALP activity and COLL1 production showed low levels at 7 d, without significant differences among groups for ALP results, and with significant higher values of COLL1 for both SrHA-containing scaffolds in comparison with HA scaffolds. At 14 d both ALP and COLL1 levels were higher than at 7 d, and significantly higher values were obtained on SrHA-containing groups than on the other groups. OPG/RANKL ratio, calculated by the value of OPG and RANKL detected in the supernatants, showed the same trend as that obtained by gene expression analysis.

It is known that Sr has a dual effect on bone remodeling: in fact, Sr not only affects osteoclast behavior, as an antiresorptive agent, but also enhances osteoblast performance.[3–6,17,18] Sr promotes bone formation inducing higher osteoblast proliferation and stimulating osteoblast activity, through different pathways, such as the activation of the Ca-sensing receptor, of MAPK and ERK signaling, and the modulation of the expression of Runx-2 gene and of the OPG/RANKL system. In particular, Sr increases the expression of OPG and decreases the one of RANKL in osteoblasts, which results as indirect role on osteoclast formation and activity.[40]

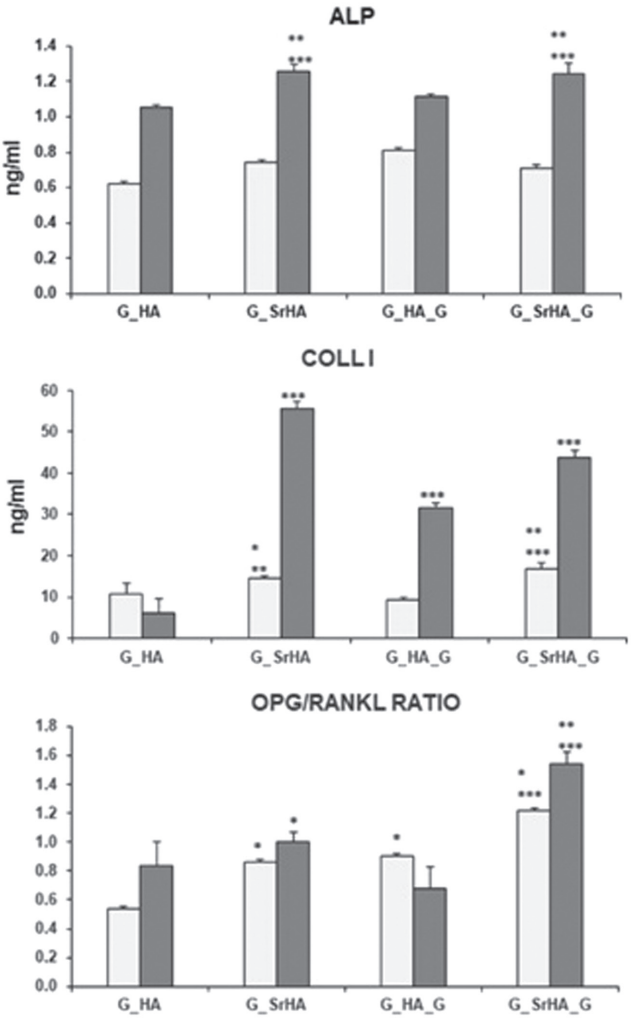

Figure 8. Immunoenzymatic assay on osteoblasts and osteoclast coculture supernatant in G_HA, G_SrHA, G_HA_G, and G_SrHA_G groups after 7 and 14 d of culture. Statistical analysis is reported in the figure (*$p < 0.05$, **$p < 0.005$, ***$p < 0.0005$). ALP. 14 d: ***G_SrHA, G_SrHA_G versus G_HA; **G_SrHA, G_SrHASr_G versus G_HA_G. COLL1. 7 d: *G_SrHA versus G_HA; **G_SrHA versus G_HA_G; **G_SrHA_G versus G_HA; ***G_SrHA_G versus G_HA_G; 14 d: ***G_SrHA versus G_HA, G_HA_G, G_SrHA_G; ***G_HA_G versus G_HA; ***G_SrHA_G versus G_HA, G_HA_G. OPG/RANKL ratio. 7 d: *G_SrHA, G_HA_G versus G_HA; *G_SrHA_G versus G_SrHA, G_HA_G; ***G_SrHA_G versus G_HA; 14 d: * G_SrHA versus G_HA_G; **G_SrHA_G versus G_SrHA; ***G_SrHA_G versus G_HA, G_HA_G.

The results of our in vitro coculture model demonstrated that strontium is able to display its anti-osteoporotic activity also when embedded as SrHA in gelatin-based scaffolds, affecting osteoclasts via both a direct action and indirect effects mediated by osteoblasts. When compared to G_HA and G_HA_G, scaffolds containing SrHA showed an enhancement of osteoblast activity and a reduction of both number and differentiation of osteoclast from monocytes precursors, mainly due to promotion of OPG expression. Reinforcement with gelatin seems to enhance the antiresorption activity of SrHA, as demonstrated by the results obtained on G_SrHA_G. This effect may be related with the higher release of Sr in culture

medium from G_SrHA_G than from G_SrHA, promoted by gelatin reinforcement, and therefore with a higher availability of Sr ions in the microenvironment of cell coculture (Figure 4).

4. Conclusions

The preparation method developed in this study allows to get biomimetic scaffolds with an open and interconnected high porosity. The pore size distribution, as well as water uptake ability and mechanical properties can be modulated through scaffold reinforcement with gelatin. Moreover, gelatin reinforcement influences strontium release from SrHA-containing scaffolds. The presence of strontium and its sustained release promote osteoblast viability and differentiation, as shown by the higher levels of ALP and COLL I, as well as by the results of gene expression, obtained for SrHA-containing scaffolds when compared to HA-containing scaffolds. On the other hand, the viability and activity of osteoclast cocultured with osteoblast are negatively affected by the presence of strontium in the scaffolds, suggesting that these systems could be usefully applied to promote bone regeneration and hinder excessive bone resorption.

Supporting Information

Supporting Information is available from the Wiley Online Library or from the author.

Acknowledgements

This research was supported by the University of Bologna. The authors are grateful to IRCCS Rizzoli Orthopaedic Institute (funds 5 X 1000 year 2015, cod. 6879).

Conflict of Interest

The authors declare no conflict of interest.

Keywords

biomimetic scaffolds, gelatin, reinforcement, strontium release

[1] P. J. Marie, P. Ammann, G. Boivin, C. Rey, *Calcif. Tissue Int.* **2001**, *69*, 121.
[2] S. G. Dahl, P. Allain, P. J. Marie, Y. Mauras, G. Boivin, P. Ammann, Y. Tsouderos, P. D. Delmas, C. Christiansen, *Bone* **2001**, *28*, 446.
[3] E. D. Deeks, S. Dhillon, *Drugs* **2010**, *70*, 733.
[4] S. J. Gallacher, T. Dixon, *Calcif. Tissue Int.* **2010**, *87*, 469.
[5] P. J. Marie, *Osteoporosis Int.* **2005**, *16*, S7.
[6] E. Bonnelye, A. Chabadel, F. Saltel, P. Jurdic, *Bone* **2008**, *42*, 129.
[7] P. Ammann, *Osteoporosis Int.* **2005**, *16*, S11.
[8] J. Y. Reginster, O. Bruyère, A. Sawicki, A. Roces-Varela, P. Fardellone, A. Roberts, J. P. Devogelaer, *Bone* **2009**, *45*, 1059.
[9] Z. Saidak, P. J. Marie, *Pharmacol. Ther.* **2012**, *136*, 216.
[10] A. Bigi, E. Boanini, M. Gazzano, in *Biomineralization and Biomaterials: Fundamentals and Applications*, 1st ed. (Eds: C. Aparicio, M. P. Ginebra), Woodhead Publishing, Cambridge, UK **2015**, p. 235.
[11] R. A. Surmenev, M. A. Surmeneva, A. A. Ivanova, *Acta Biomater.* **2014**, *10*, 557.
[12] G. Graziani, M. Bianchi, E. Sassoni, A. Russo, M. Marcacci, *Mater. Sci. Eng., C* **2017**, *74*, 219.
[13] S. Tadier, R. Bareille, R. Siadous, O. Marsan, C. Charvillat, S. Cazalbou, J. Amédé, C. Rey, C. Combes, *J. Biomed. Mater. Res., Part B* **2012**, *100*, 378.
[14] M. P. Ginebra, C. Canal, M. Espanol, D. Pastorino, E. B. Montufar, *Adv. Drug Delivery Rev.* **2012**, *64*, 1090.
[15] M. Schumacher, M. Gelinsky, *J. Mater. Chem. B* **2015**, *3*, 4626.
[16] W. Xue, H. L. Hosick, A. Bandyopadhyay, S. Bose, C. Ding, K. D. K. Luk, K. M. C. Cheung, W. W. Lu, *Surf. Coat. Technol.* **2007**, *201*, 4685.
[17] C. Capuccini, P. Torricelli, F. Sima, E. Boanini, C. Ristoscu, B. Bracci, G. Socol, M. Fini, I. N. Mihailescu, A. Bigi, *Acta Biomater.* **2008**, *4*, 1885.
[18] C. Capuccini, P. Torricelli, E. Boanini, M. Gazzano, R. Giardino, A. Bigi, *J. Biomed. Mater. Res., Part A* **2009**, *89*, 594.
[19] B. Bracci, P. Torricelli, S. Panzavolta, E. Boanini, R. Giardino, A. Bigi, *J. Inorg. Biochem.* **2009**, *103*, 1666.
[20] W. Zhang, Y. Shen, H. Pan, K. Lin, X. Liu, B. W. Darvell, W. W. Lu, J. Chang, L. Deng, D. Wang, W. Huang, *Acta Biomater.* **2011**, *7*, 800.
[21] C. Lindahl, S. Pujari-Palmer, A. Hoess, M. Ott, H. Engqvist, W. Xia, *Mater. Sci. Eng., C* **2015**, *53*, 322.
[22] E. Landi, A. Tampieri, G. Celotti, S. Sprio, M. Sandri, G. Logroscino, *Acta Biomater.* **2007**, *3*, 961.
[23] Z. Xu, Y. Lei, W. Yin, Y. Chen, Q. Ke, Y. Guo, C. Zhang, *J. Mater. Chem. B* **2016**, *4*, 7919.
[24] Y. Lei, Z. Xu, Q. Ke, W. Yin, Y. Chen, C. Zhang, Ya. Guo, *Mater. Sci. Eng., C* **2017**, *72*, 134.
[25] C. Ehret, R. Aid-Launais, T. Sagardoy, R. Siadous, R. Bareille, S. Rey, S. Pechev, L. Etienne, J. Kalisky, E. de Mones, D. Letourneur, J. A. Vilamitjana, *PLoS One* **2017**, *12*, e0184663.
[26] Y. Li, Q. Li, S. Zhu, E. Luo, J. Li, G. Feng, Y. Liao, J. Hu, *Biomaterials* **2010**, *31*, 9006.
[27] C. M. Murphy, M. G. Haugh, F. J. O'Brien, *Biomaterials* **2010**, *31*, 461.
[28] R. A. Perez, G. Mestres, *Mater. Sci. Eng., C* **2016**, *61*, 922.
[29] S. Amadori, P. Torricelli, K. Rubini, M. Fini, S. Panzavolta, A. Bigi, *J. Mater. Sci.: Mater. Med.* **2015**, *26*, 69.
[30] S. Panzavolta, P. Torricelli, S. Casolari, A. Parrilli, S. Amadori, M. Fini, A. Bigi, *Macromol. Biosci.* **2017**, *17*, 1600272.
[31] A. Bigi, E. Boanini, C. Capuccini, M. Gazzano, *Inorg. Chim. Acta* **2007**, *360*, 1009.
[32] J. Terra, E. R. Dourado, J. G. Eon, D. E. Ellis, G. Gonzalez, A. M. Rossi, *Phys. Chem. Chem. Phys.* **2009**, *11*, 568.
[33] H. B. Pan, Z. Y. Li, W. M. Lam, J. C. Wong, B. W. Darvell, K. D. K. Luk, W. W. Lu, *Acta Biomater.* **2009**, *5*, 1678.
[34] G. X. Ni, B. Shu, G. Huang, W. W. Lu, H. B. Pan, *J. Biomed. Mater. Res., Part B* **2012**, *100*, 562.
[35] S. Amadori, P. Torricelli, S. Panzavolta, A. Parrilli, M. Fini, A. Bigi, *Macromol. Biosci.* **2015**, *14*, 941.
[36] V. Karageorgiou, D. Kaplan, *Biomaterials* **2005**, *26*, 5474.
[37] S. Panzavolta, P. Torricelli, S. Amadori, A. Parrilli, K. Rubini, E. Della Bella, M. Fini, A. Bigi, *J. Biomed. Mater. Res., Part A* **2013**, *101*, 3560.
[38] S. Amadori, P. Torricelli, S. Panzavolta, A. Parrilli, M. Fini, M. A. Bigi, *Macromol. Biosci.* **2015**, *15*, 1535.
[39] W. Querido, A. L. Rossi, M. Farina, *Micron* **2017**, *80*, 122.
[40] M. Pilmane, K. Salma-Ancane, D. Loca, J. Locs, L. Berzina-Cimdina, *Mater. Sci. Eng., C* **2017**, *78*, 1222.